Circular Distribution of Corona Current of Multiple-Conductor Transmission Line (Ⅳ)

Saburo MUTO, Tsuginori INABA and Toshio SHIBATA

Department of Electrical Engineering

(Received September 11, 1967)

This paper is the 4th about characteristics of D. C. corona current circular distribution of multiple conductor transmission line in order to settle multiple conductors in E. H. V. cables with compressed gas. Gases used under investigation were SF_6, CO_2, N_2, etc. and the pressure range was from 10 Torr to 7 kg/cm^2 abs. Distribution and directivity factor of corona current and corona starting voltages were measured and discussed.

1. Introduction

The authors have made a study of this subject and already published the results of the investigation under the same title in the Bulletin of Nagoya Institute of Technology.[1]~[3] The lst report dealt with the mean corona loss-angle θ_m of a multiple-conductor transmission line in air and the shielding effect when one of the double-conductors was coated with insulating material. In the 2nd report we have described in detail the shielding effects on the double-conductor in combination with a brass-wire and a P. V. C. coated-wire. And in the 3rd report the corona starting voltage, the distribution and the directivity of the corona current on the double-conductors at low air pressure, lower than 1 atm., were reported, when an air-sealed coaxial cylindrical-electrode equipment was used, in which the gas pressure was easily adjustable.

The contents of the 4th report are as follows.

(1) Almost the same equipment was used as in the 3rd report.

(2) Pressure range: 10 Torr to 7 kg/cm^2 abs., mainly at 1 kg/cm^2 abs. or more.

(3) Gases used: Air, N_2, CO_2 and SF_6.

(4) Measurement of corona starting voltage, circular distribution and directivity factor of corona current.

(5) Introduction of a mathematical model of corona current distribution and the analysis of the critical corona angle.

The purpose of this paper is to make a comparison of the differences between the characteristics of the corona current distribution on the double-conductors in various gases. The electronegative gases, such as SF_6 for insulant, are now under investigation.

2. Experimental Apparatus and Measuring Method

The description of measuring equipment is omitted here, because the details are the same with Fig. 1-A in the reference (3). However, in this case, 36 Al-electrodes of 0.02 mm thickness was used instead of previous 36 piano-wire electrodes of 0.3 mmϕ as measuring electrodes, to avoid the bending tendency of a piano-wire which was not suitable for theoretical calculation of the electric field. The difference of the corona starting voltage in both cases was negligible.

Fig. 1 shows the measuring circuit. The maximum output voltage is D. C. ±70KV.

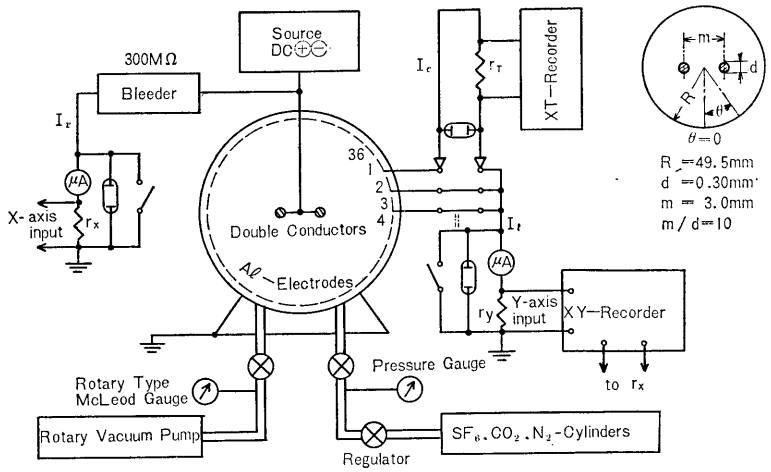

Fig. 1 Measuring Circuit.

Two piano wires of 0.3 mmϕ each were located parallel to each other with 3 mm spacing for double-conductors in the previous papers. The principal dimensions of the equipment are as follows.

$N=2$, $m/d=10$, $d=0.3$mmϕ, $R=49.5$mm,

where N: number of conductors.

m: spacing between two conductors.

d: diameter of conductor.

R: inner radius of cylindrical electrode.

A micro-micro ammeter and a X-Y Recorder were used to measure the corona starting voltage. The bleeder-current I_r as a function of the applied voltage, was fed into the X-axis of the X-Y Recorder, and the total corona current I_t into the Y-axis. The corona starting voltage is defined as the value corresponding to the abruptly increasing point of I_t. One standard resistance r_T, 20 to 2000 Ω, was inserted in each measuring terminal of electrodes. And then the terminal voltage of r_T was recorded with X-T Recorder by potentiometer-method as a function of peripheral angle corresponding to the time-scale of the X-T Recorder.

During measurement, all the rest of the electrodes were grounded. The characteristics were measured in the range of 10 Torr up to 7 kg/cm² abs.

Table. 1 Purities of Supplied Gases.

	N_2	CO_2	SF_6
Purity (%)	99	99.98 (volume)	99.95
Water (p.p.m.)	——	4 max. (weight)	7.9max.

3. Corona Starting Voltage

3-1. Calculation of Surface Gradients

At the coaxicial cylindrical electrode in air, the corona starting potential gradient E_s, which was investigated by Watson et al., is given by the following experimental equation.

$$E_s=Am_1\delta(1+C/\sqrt{\delta r})\ [\mathrm{KV/cm}],\cdots\cdots(3.1.1)$$

where A and C are the constants determined by the polarity, r radius of curvature of the conductor in cm, δ relative air density and m_1 coefficient of surface condition.

The maximum surface gradient, E_{max}, of the double-conductor of this experimental apparatus is given as follows. (See Appendix.)

$$E_{max}=8.49V\ [\mathrm{KV/cm}],\cdots\cdots(3.1.2)$$

where V is the supplied voltage in kilovolts. The corona starting voltage V_s is obtained by the condition of $E_s=E_{max}$ as

$$V_s=Am_1\delta(1+C/\sqrt{\delta r})/8.49\ [\mathrm{KV}].\cdots\cdots(3.1.3)$$

Table 2 shows the calculated values with the

Table. 2 Comparison of Corona Starting Voltages in Air at 1 atm.

Model	$\frac{m}{d}$ [cm]	Voltage Polarity	Constants[4] A	Constants[4] C	Temp. [°C]	δ	Vs [KV] Calculated	Vs [KV] Measured	Deviation [%]
I	$\frac{0.300}{0.030}$	Positive	33.7	0.241	10.8	1.050	12.2	12.7	+ 3.9
		Negative	31.0	0.308	10.0	1.053	13.27	12.95	− 2.4
II*	$\frac{0.705}{0.081}$	Positive	33.7	0.241	14.0	1.038	18.88	18.86	− 0.1

$m_1=1$, Positive: Watson's const., Negative: Whitehead's const.

* Model II was only used to evaluate the experimental accuracy.

constants, A and C, by Watson et al. and our experimental values. The difference of measured and calculated values was within 3 % range at Model I and within 0.1 % at Model II.

3-2. Corona Starting Voltage in Several Gases

(1) Corona starting voltage at low pressure (10 to 800 Torr).

Fig. 2 shows the V_s-pressure characteristics at low pressure. The characteristic curve of V_s in Fig. 2, when the conductor potential is negative (notation⊖), crosses the line in the positive (notation⊕) in air at near 100 and 800 Torr. The P-V_s in air shows $V_s⊖ > V_s⊕$ at 1 atm. This characteristic could not be observed in other gases, and the corona starting voltage of ⊖ is always lower than that of ⊕. The difference between positive and negative V_s in SF_6 is smaller at 100 Torr or less. At the high pressure more than 100 Torr, $V_s⊕SF_6$ is 1.6 to 1.8 times as large as $V_s⊖SF_6$. The ratio of $V_sCO_2⊕$ to $CO_2⊖$ is 1.12 to 1.18. V_s of N_2 shows only one point at 1 kg/cm² abs. because of the complexity of the figure.

(2) Corona starting voltage at high pressure (1 to 7 kg/cm² abs.).

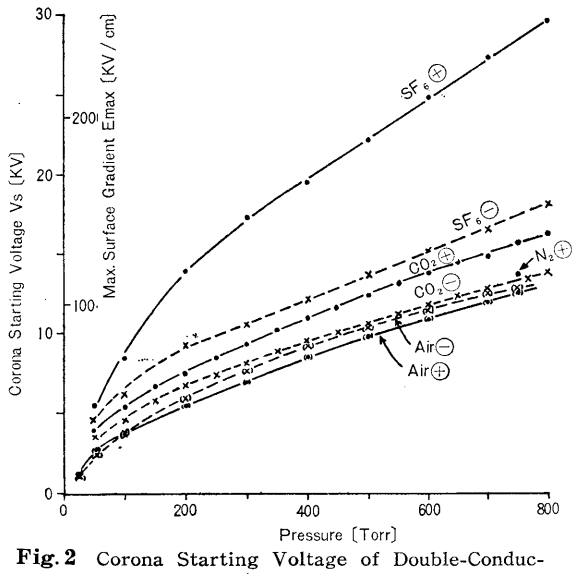

Fig. 2 Corona Starting Voltage of Double-Conductors at Low Pressure.
$N=2$, $m/d=10$, $d=0.3^{mm\phi}$.

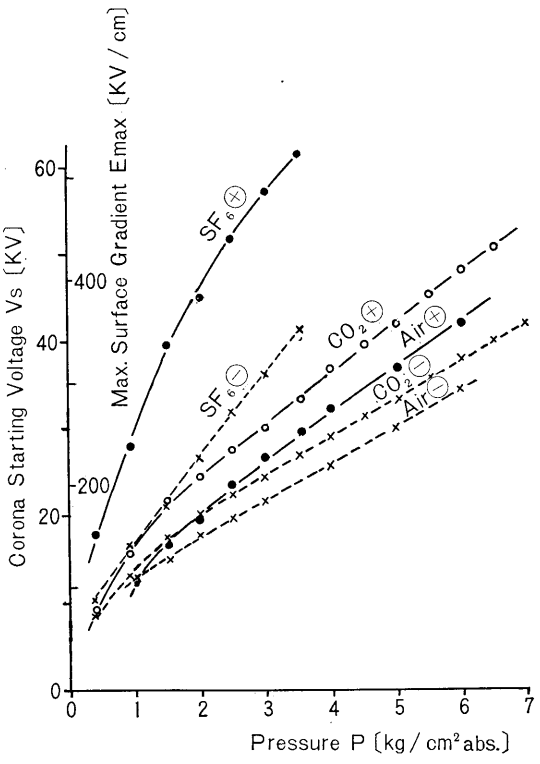

Fig. 3 Corona Starting Voltage of Double-Conductors at High Pressure.
$N=2$, $m/d=10$, $d=0.3^{mm\phi}$.

On the corona starting characteristics at high pressure (Fig. 3), the difference between gases is not recognized so clearly as at low pressure. $V_s\oplus$ in air exceeds $V_s\ominus CO_2$ near 2 kg/cm² abs. V_s's of $\oplus$ in CO_2 and air, $\ominus$ in CO_2 and air, respectively, ascend in parallel with each other in the increase of pressure and the ratio between V_s's of the same polarity draws to 1. On the other hand, $V_s\oplus$ and $V_s\ominus$ of each gas ascends with constant ratio as the pressure increases in general. The ratio of $V_s\oplus$ to $V_s\ominus$ equals 1.7~1.5 in SF_6, but in CO_2, air and N_2 is 1.17~1.30. These curves are approximately written as $\ln V_s = a + b \ln P$ (P : pressure) under the 3 kg/cm² abs. and as $V_s = a' + b'P$ over the 3 kg/cm² abs.

4. Characteristics of D. C. Corona Current in N_2 Gas

4-1. Circular Distribution in N_2 Gas

The characteristics of corona current around double-conductors in N_2 are very different between $\oplus$ and $\ominus$. Fig. 4 shows an example of the distributions. The distribution in $\oplus$ is very stable. But in $\ominus$, the distribution changes so violently in time that one varies on each measurement. These characteristics seem to suggest the inverse phenomena described in the latter. To maintain the constant corona current, the applied positive voltage must be increased slightly in time as the results of the suppression effect of space charge. In negative, reversely, the corona current increases rapidly in time by their negative characteristics.

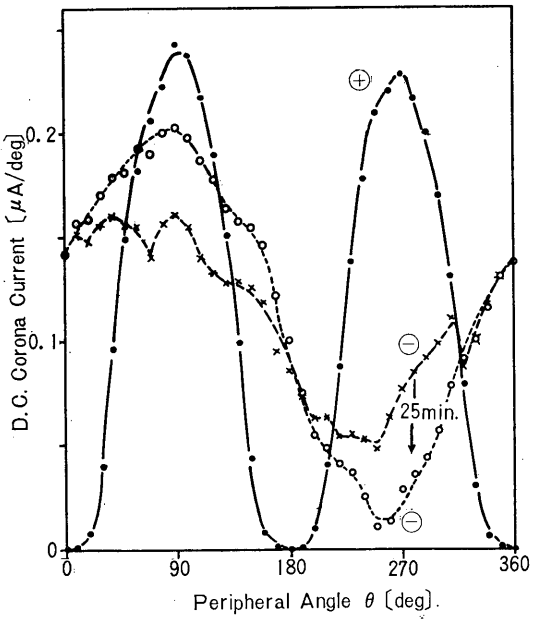

Fig. 4 Circular Distribution of D. C. Corona Current of Double-Conductors in N_2 Gas.
$N=2$, $m/d=10$, $P=1$ kg/cm² abs., $I_t=40\mu A$.

4-2. Directivity Factor in N_2 Gas

We adopted the directivity factor to analyze the corona current distribution.

Directivity factor $\kappa = \dfrac{I_{max}}{I_{min}}$

where I_{max}: corona current of the electrode elements corresponding to $\theta = 90°$ and 270°, in the direction of maximum surface gradient of the double-conductor.

I_{min}: current through the electrode elements of $\theta = 0°$ and 180°.

Fig. 5 shows the directivity factor κ of N_2 $\oplus$. The characteristics of $I_t - \kappa$ curve at $P=1$ kg/cm² abs. are separated into two regions at ca. 300μA. In region I with scre-

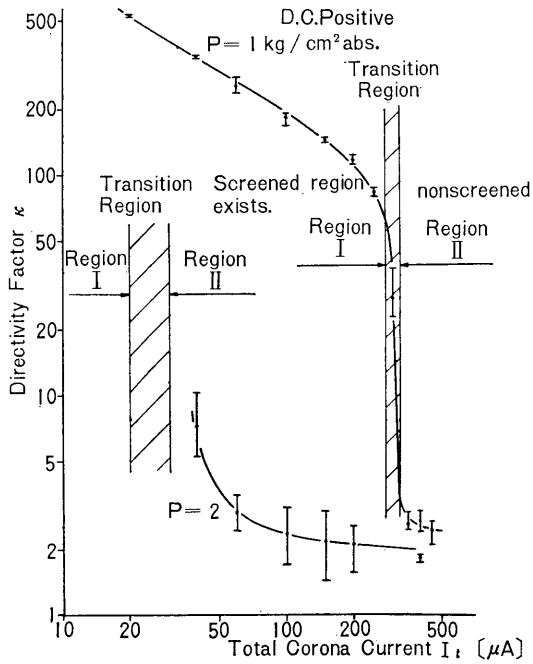

Fig. 5 κ vs. I_t in N_2 Gas.

ened area, there is an extremely high point of κ more than 100. In region Ⅱ, $I_t>300\mu A$, the screened area disappeared and the κ fell down rapidly under 10, then the total corona current contained pulses.

In the range over the $I_t=500\mu A$ point, the measurement was not taken for fear that sparks might be caused by a V-I_t curve.

At $P=2\,kg/cm^2$ abs. the corona current in region Ⅰ was so very unstable that we could not measure κ accurately. But the screened region was observed as at $P=1$. In this case the transition region was located between $I_t=20\sim30\mu A$. In region Ⅱ the corona current became quite stable. The value of κ is lower than at $P=1$. In the large current region over five hundred μA or more, each value of κ approaches the same gradually. But κ in $N_2\ominus$ could not be accurately obtained because of the unstable characteristics.

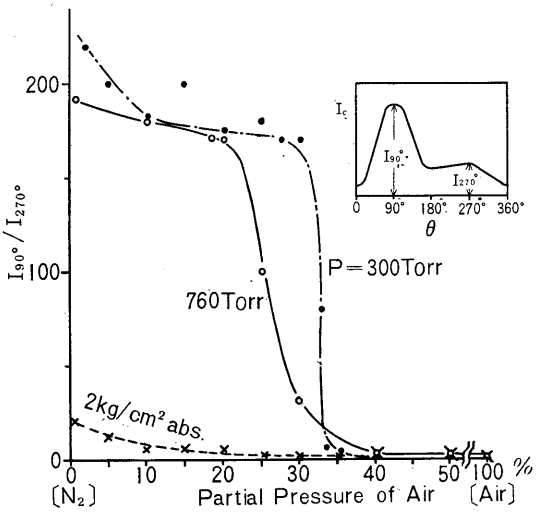

Fig. 6 Improvement of Instability of D. C. Negative Corona Current of Double-Conductors in N_2-Air mixed Gas.[5]
$N=2$, $m/d=10$, $I_t=300\mu A$.

In mixed N_2 with air,[5] the distribution of corona current becomes regular and the irregularity at the crest disappears. It is shown in Fig. 6.

5. Characteristics of D. C. Corona Current in CO_2 Gas

5-1. Circular Distribution in CO_2 Gas

The corona current distribution in CO_2 is regular and stable. Fig. 7 shows an example of the distribution. The $\oplus$ forms a twin-circular figure; we can show it over the whole measurement of I_t. The distribution of $\ominus$ becomes nearly elliptic. In this case, of course, the outside extent of corona current distribution also appears toward $\theta=90°$

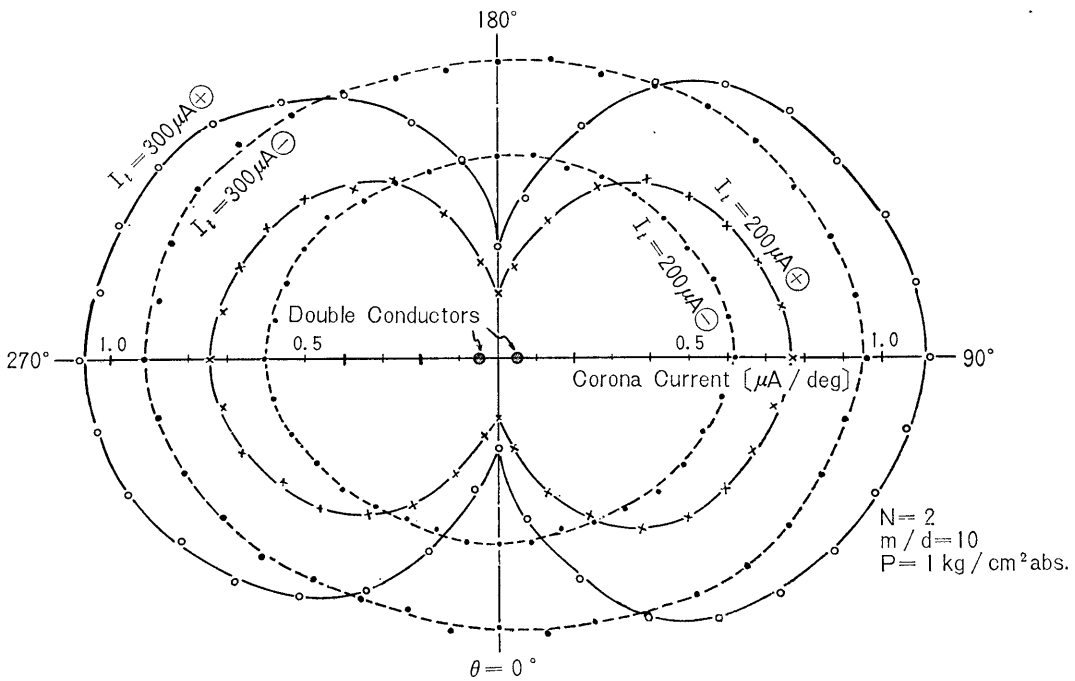

Fig. 7 Circular Distribution of D. C. Corona Current of Double-Conductors in CO_2 Gas.

and 270°. The magnitude of the extent, however, is relatively small. This is the common tendency with the negative current.

5-2. Directivity Factor in CO_2 Gas

The directivity factor κ of positive in CO_2 decreases in inverse proportion to the applied voltage, but increases with pressure.[6][7] In decreasing I_t all of these characteristics have a tendency to sharpen the directivity of corona current. The characteristics of I_t-κ curves in Fig. 8 show the above tendency clearly. The characteristics are expressed by $log\kappa = a - blogI_t$. It is very interesting to note that these straight lines seem to cross

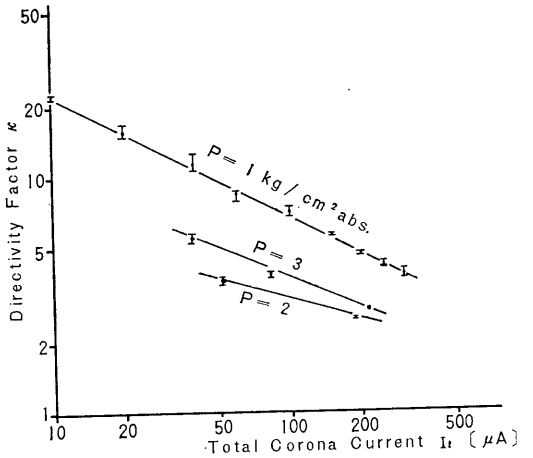

Fig. 8 Directivity Factors of D. C. Corona Current of Double-Conductors in CO_2 Gas.
$N=2$, $m/d=10$.
(a) D. C. Positive.

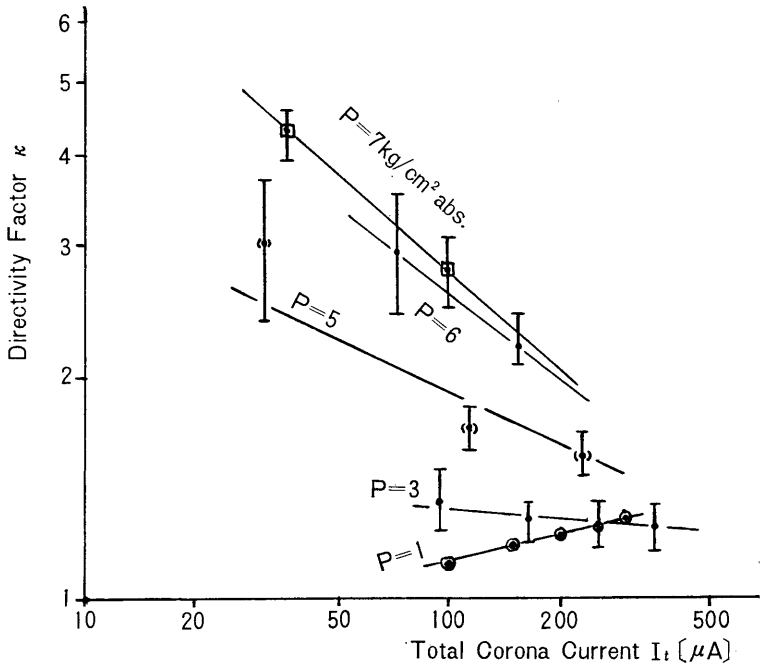

(b) D. C. Negative.

at $\kappa \fallingdotseq 1$ in a large current region.

6. Characteristics of D. C. Corona Current in SF_6 Gas

6-1. Circular Distribution in SF_6 Gas

Fig. 9-(a) indicates the corona current distribution at 50 KV constant in SF_6. The corona current descends rapidly in reverse proportion to the pressure, because the discharge is suppressed owing to the electron attachment and the absorption coefficient of photon. It is recognized that the corona current distribution is very different in ⊕ and ⊖. In Fig. 9, only one half is shown because the two-parts are symmetrical. In ⊕ the distribution curves of corona current are of the so-called cocoon type, but in ⊖ the curves are of the twin-circle forms as of CO_2 ⊕. These tendencies are also recognized in the case of constant pressure. Fig. 9-(b) shows the corona distribution at

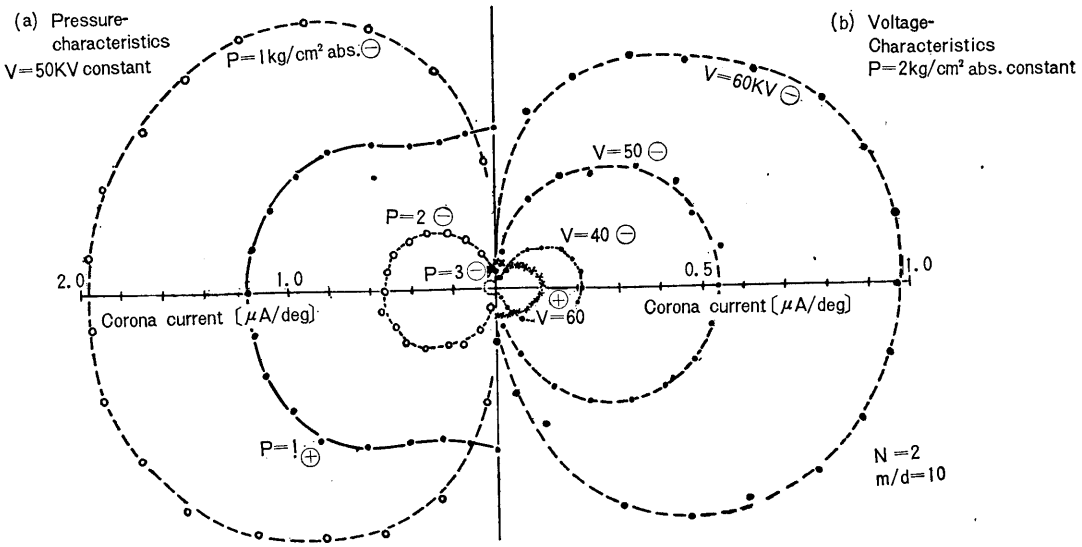

Fig. 9 Circular Distribution of D. C. Corona Current of Double-Conductors in SF_6 Gas.

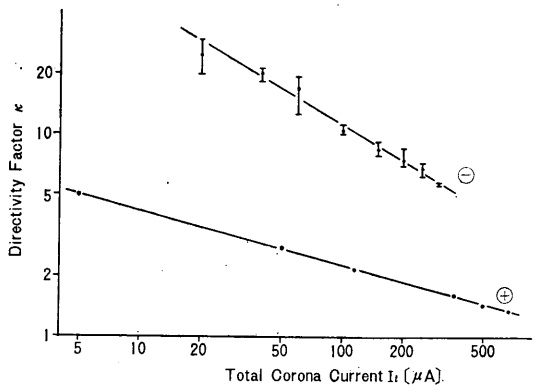

Fig. 10 Directivity Factor of D. C. Corona Current of Double-Conductors in SF_6 Gas. $N=2$, $m/d=10$, $P=1$kg/cm² abs.

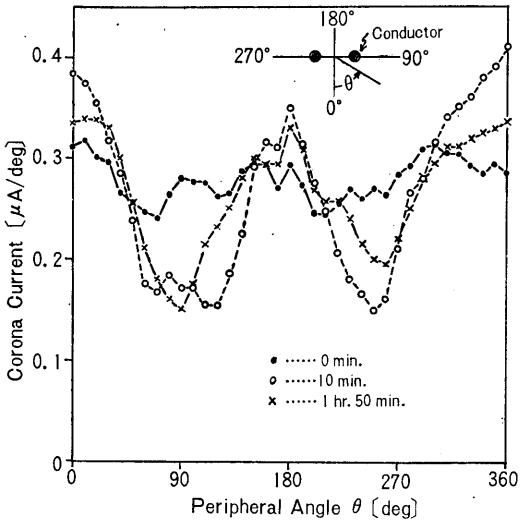

Fig. 11 Time-Variation of Inverse Corona Current Distribution of Double-Conductors in SF_6 Gas.
$N=2$, $m/d=10$, $P=2$ kg/cm² abs., $V=50$ KV⊖.

$P=2$ kg/cm² abs. The total corona current in ⊕ is considerably smaller, because the corona starting voltage of ⊕ is somewhat larger than of ⊖.

6-2. Directivity Factor in SF_6 Gas

It was previously reported that the κ in SF_6 decreased with increasing applied voltage in both ⊕ and ⊖. But if the pressure was increased, κ increased at a constant voltage. Fig. 10 shows the I_t-κ characteristics at 1 kg/cm² abs. κ is small in the positive, but large in the negative. This relation of $\kappa\oplus<\kappa\ominus$ in SF_6 was in the inverse relation in CO_2. The experimental formulas are as follows.

$$\kappa \cdot I_t^B = A \quad \cdots\cdots (6.2.1)$$

where in ⊕ case $A=7.61$, $B=0.270$ and in ⊖ case $A=171$, $B=0.603$.

7. Inverse Phenomena of Circular Distribution

We observed at times the inverse distribution of corona current, rotating 90° from

the normal form.

In Fig. 11 the chart gives an example under the condition of 50 KV⊖ constant in SF_6. After obtaining the more or less flat-like single circle distribution immediately after applying the voltage, the valleys of inverse phenomena developed towards $\theta=90°$ and 270° where the crests should appear. The valleys gradually became deep with the passage of a short period. After 10 minutes or so the inverse phenomena became stable and the distribution was continued for 2 hours or more. These phenomena arose at 45 KV⊖, too.

On the other hand, unstable distribution in N_2 ⊖, which changes rapidly in a short time, has no fixed points at which valleys arise. Consequently those in N_2 can be clearly distinguished from the inverse phenomena in SF_6⊖. The reason for the inverse phenomena in SF_6 seems to be caused by its large attachment coefficient.

8. Analysis of Circular Distribution of Corona Current

8-1. One of the Mathematical Models of Circular Distribution

Many distributions of corona current have been discussed, such as the twin-circular type, the cocoon type and others. These types are determined by the kinds of gases, pressure, polarity and range of corona current. The Booth's curves are introduced then to unify those types, and shown in polar coordinates as follows.

$$r^2=b^2-4a^2\sin^2\theta \quad \cdots\cdots(8.1.1)$$

Fig. 12 shows the forms in Eq. (8.1.1), which are classified as follows.

(1) $b<2a$: lemniscatelike type
(2) $b=2a$: twin-circular type
(3) $b>2a$: cocoon type
(4) $b\gg 2a$: elliptic type
(5) $b\gg 2a$: single-circular type

These figures are relatively suitable for showing experimental results.

The lemniscatelike type corresponds to the distribution in N_2⊕; the twin-circular type to the general form; the cocoon type to the ascending-valley form; the elliptic type to in CO_2⊖ and the single circular type to preinverse phenomena.

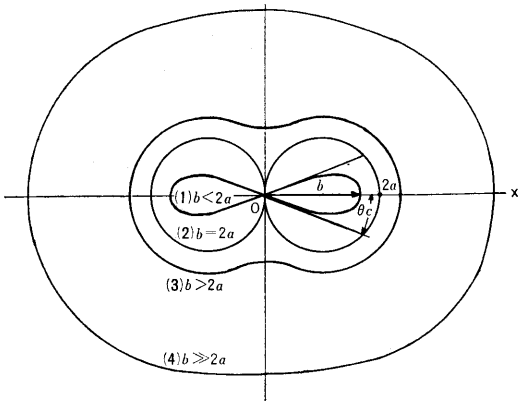

Fig. 12 Booth's Curves.

The directivity factor is infinite in (1) and (2) theoretically, and can be defined only in the range of $b>2a$. The directivity factor of Booth's curve, κ_B, is given as follows.

$$\theta=0° : r_{max}=I_{max}=b \quad \cdots\cdots(8.1.2)$$

$$\theta=90° : r_{min}=I_{min}=\sqrt{b^2-4a^2} \quad \cdots\cdots(8.1.3)$$

$$\kappa_B=r_{max}/r_{min}=b/\sqrt{b^2-4a^2}$$
$$=1/\sqrt{1-(2a/b)^2} \quad \cdots\cdots(8.1.4)$$

And the total corona current I_{tB} is

$$I_{tB}=\int_0^{2\pi} r\,d\theta=b\int_0^{2\pi}\sqrt{1-(2a/b)^2\sin^2\theta}\,d\theta$$
$$=4b\cdot E(2a/b) \quad \cdots\cdots(8.1.5)$$

where E $(2a/b)$ is complete elliptic integral. Therefore the relation between κ_B and I_{tB} is

$$I_{tB}=4I_{maxB}E(\sqrt{1-1/\kappa_B{}^2}) \quad \cdots\cdots(8.1.6)$$

or $$\kappa_B=\left[1-\{E^{-1}(I_{tB}/4I_{maxB})\}^2\right]^{-\frac{1}{2}} \quad \cdots\cdots(8.1.7)$$

On the other hand, the experimental formula is

$$\kappa\cdot I_t{}^B=A \quad \cdots\cdots(8.1.8)$$

where A and B are constants determined by the kinds of gases, pressure, polarity, etc. We are investigating in order to draw out better mathematical models of it.

8-2. Analysis of Critical Corona Angle

Critical corona angle θ_c is defined as the angle between the X-axis and the tangent

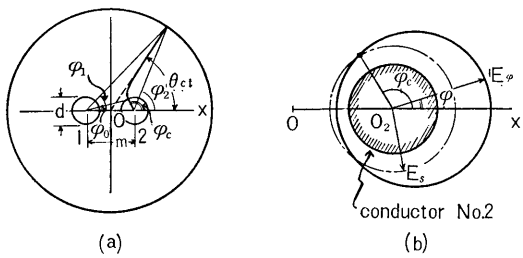

Fig. 13 Schematic Diagram of Electric Field.

line through the center point of lemniscate-like form. In the static theory the corona current should be zero in the range of $\theta > \theta_c$, but actually small current does exist. The surface potential gradient $E\varphi$ on angle φ shown in Fig. 13-(b) is written as follows.

$$\left.\begin{aligned} &E\varphi = E_{max}(1+\lambda\cos\varphi)/(1+\lambda), \\ &\lambda = 1/\{(m/d)+0.72\} \end{aligned}\right\} \cdots\cdots (8.2.1)$$

If the corona starting gradient is noted as E_s, $E_\varphi = E_s$ gives the boundary angle of corona creating region. This φ is called the critical corona angle φ_c and written as follows.

$$\varphi_c = \cos^{-1}\{(E_s/E_{max})(1+1/\lambda) - 1/\lambda\} \cdots\cdots (8.2.2)$$

Using the bleeder current I_v instead of E_s and E_{max}, the above equation is changed into

$$\varphi_c = \cos^{-1}\{(I_{vs}/I_v)(1+1/\lambda) - 1/\lambda\} \cdots\cdots (8.2.3)$$

where I_{vs} is the bleeder current at corona starting and I_v at measuring φ. The surface charge of a double-conductor ($m/d=10$) can be regarded as parallel equipotential lines of charge. Therefore the electric line of force in the static field before corona is obtained as follows.

$$\varphi_1 + \varphi_2 = \text{constant} \cdots\cdots (8.2.4)$$

where φ_1 and φ_2 are shown in Fig. 13-(a).

The theoretic critical corona angle without space charge θ_{cto} is defined as the angle of cylindrical electrode where the electric lines of force come out of the angle φ_c on the conductor surface.

$$\theta_{cto} = (\varphi_c + \varphi_0)/2 \cdots\cdots (8.2.5)$$

$$\varphi_0 = \tan^{-1}\left[\{(d/2)\sin\varphi_c\}/\{m+(d/2)\cos\varphi_c\}\right] \fallingdotseq (\sin\varphi_c)(180/\pi)/\{(2m/d)+\cos\varphi_c\} \text{ [deg]} \cdots\cdots (8.2.6)$$

Fig. 14 shows θ_{cto} and θ_{cm}, which was measured in the case of $N_2\oplus$ at 1 kg/cm² abs. which had clearly screened off areas. θ_{cm} was read from distribution on Cartesian coordinates. The difference between θ_{cm} and θ_{cto} is caused by the diffusion and repulsive effects of space charge. The difference is almost constant up to $I_t = 5\mu A$, and at more than $5\mu A$ it decreases linearly with increasing I_t. The large deflection of the angle in a region of small I_t is due to the effects of the repulsion and the like, by the space charge produced in the small area. This result is twice the amount of the calculated value. But in region of large I_t, it seems that the amount of space charge near $\varphi = 0$ affects the deflection only a little at the point of φ far from $\varphi = 0$.

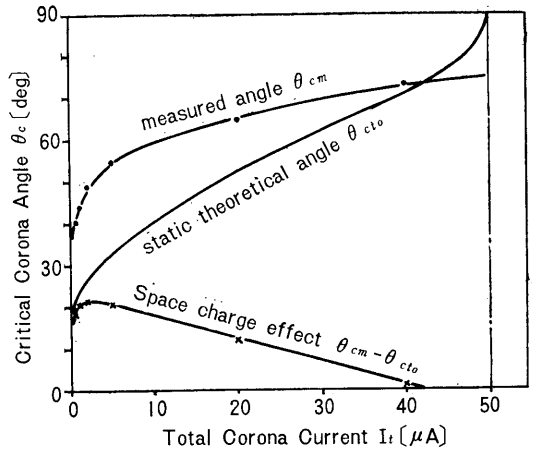

Fig. 14 Critical Corona Angle and Space Charge Effect.
$N=2$, $m/d=10$, $P=1\text{kg/cm}^2$ abs., $N_2\oplus$.

8-3. Analysis of the Directivity Factor

It is recognized that the directivity factors κ change under various conditions. The κ in the negative case is described qualitatively as follows. By the corona dischage in $E(r, \varphi) > E_s$ or $r_c < r < r_b(\varphi)$, which produces positive ions (M^+) and electrons (e^-) as shown in Fig. 15, M^+ goes toward the conductors and e^- toward the cylindrical electrodes. e^- is not influenced in the layer of the corona discharge ($r < r_b(\varphi)$) by the canceling effect in M^+ and e^-. After e^- gets out of $r_b(\varphi)$, where electrons exist only, cohesion between

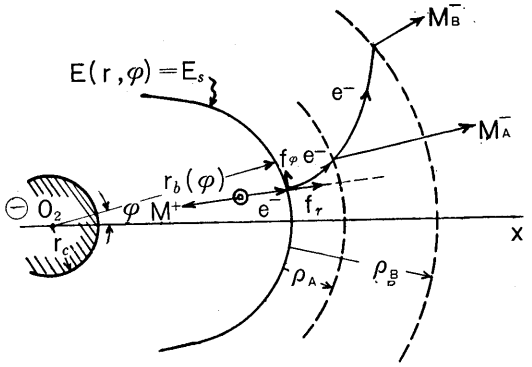

Fig. 15 Trajectories of Negative Carriers.

the electrons decreases. The forces on e^- are separated into two forces: f_r by the electric field, and f_φ by the synthetic force of the repulsive action. The trajectory of e^- shown in Fig. 15 is deflected to the φ increasing. e^- cannot reach the electrodes directly, but they attach themselves to neutral gas molecules in negative ion M^- after many impacts. Then e^- goes on as M^- toward the electrodes. The electron attachment path of e^- to SF_6, ρ, is small with large attachment coefficient η and it varies in inverse proportion to the gas density n.

For example in gases A and B is $\eta_A > \eta_B$, the relation of ρ is $\rho_A < \rho_B$ and e^- in gas B is deflected laterally more than in gas A. Consequently, the smaller the η, the smaller the κ. In $P_A < P_B$, $n_A < n_B$ results $\rho_A > \rho_B$, then $\kappa_A < \kappa_B$. Therefore the κ increases with pressure.

As the reason of decreasing κ with increasing I_t, in addition to the lateral expansion effect, the decreasing relative variation on φ of $(E-E_s)$ is also pointed out.

9. Conclusions

(1) The directivity factor κ which decreases generally as increment of total corona current I_t, can be written as the experimental equation of $\kappa \cdot I_t^B = A$, where A and B are the constants determined by kind and pressure of gases, polarity and region of I_t.

(2) Under the same conditions the κ's positive ⊕ in air, N_2 and CO_2 were higher than negative ⊖. However, κ in SF_6, a strong electronegative gas, was opposite.

(3) Under the applied voltage constant, κ in ⊕ and ⊖ increased always with the pressure. Under I_t constant, in negative in air, CO_2 and SF_6, the κ increased always with the pressure, but in positive in N_2, CO_2 and SF_6, κ at 2 kg/cm² abs. was lower than that at 1 kg/cm² abs.

(4) In N_2⊕ the region I with a screened area was clearly observed. In this region κ was more than 100 and in region Ⅱ with non-screened area less than 10. The corona distribution in region I was lemniscatelike type and in Ⅱ twin-circular type. The distribution ⊖ was on great change in time and the valleys appeared almost at unexpected area.

(5) In CO_2, the distribution ⊕ with the high κ was twin-circular type and in ⊖ with the low κ, elliptic type.

Table. 3 Corona Current Distribution Forms in Various Gases at 1kg/cm² abs.

Directivity factor κ			∞ ←				1	
Polarity	Attachment	Gas	lemniscate	twin-circle	cocoon type	elliptic type	single-circle	unstable
Negative	↓ strong	N_2						←→
		CO_2				←→		
		SF_6		←→				
Positive	↓ strong	N_2	region I ←→	region Ⅱ ←→				
		CO_2		←→				
		SF_6			←→			

(6) In SF_6, the distribution ⊕ with the low κ was so-called cocoon type and ⊖ with the high κ, twin-circular type.

(7) From Table 3, we can recognize that κ⊖ increases with attachment coefficients of gases, but κ⊕ decreases.

(8) The inverse phenomena of the distribution were observed only in SF_6 ⊖.

(9) It was pointed out that Booth's curves were suitable for one of the mathematical models of the corona current distributions.

(10) In analysis of critical corona angle without space charge, it was known that the lateral expansion effect of the corona current distribution decreased with the increment of I_t.

Acknowledgements

The authors wish to thank Mr. Tatsuo Tani (Electrotechnical Laboratory of Japan), Mr. K. Nakamura, Mr. S. Kozu and Mr. M. Udaka for their help and cooperation.

Appendix

Surface Potential Gradients on Multiple-Conductor. In general the maximum surface gradient E_{nmax} of n-bundled conductors arranged in a regular polygon, is given as follows.

$$\left.\begin{aligned} E_{nmax}&=V\left\{1+(n-1)\frac{d}{m}\sin\frac{\pi}{n}\right\}/nr\ln(R/R_e)\ \text{〔KV/cm〕},\\ R_e&=\sqrt[n]{rm_e^{n-1}},\qquad m_e=\sqrt[n-1]{\prod_{j=1}^{n-1}m_{nj}},\end{aligned}\right\}\quad\cdots\cdots(1)$$

where $d=2r$ is diameter of each conductor, R distance between the center of multiple-conductor and grounded electrodes, R_e radius of the equivalent single conductor, m spacing between the adjoining conductors, m_e equivalent spacing between conductors and m_{nj} distance between the centers of the n th and the j th conductors, all in cm.

By inserting the dimensions of this apparatus into Equation (1), E_{nmax} becomes using a compensating term[8][9]

$$E_{max}=3.49V\ \text{〔KV/cm〕}.\quad\cdots\cdots(2)$$

References

(1) S. Muto: Bulletin of Nagoya Institute of Technology vol. 15 pp. 253-258 (1963)

(2) S. Muto: ibid. vol. 16 pp. 264-268 (1964)

(3) S. Muto & T. Tani: ibid. vol. 17 pp. 246-254 (1965)

(4) Handbook of Discharge p. 110 I. E. E. of Japan (1958)

(5) S. Muto & T, Tani: Trans. of the 1966 Joint Convention of the 4 Electrical Institutes, Japan, paper No. 765 (1966)

(6) S. Muto & T. Inaba: Journal of J. R. E. D. No. 29 p. 135 (1967)

(7) S. Muto, T. Inaba & S. Kozu: Trans. of the 1967 Joint Convention of the 4 Electrical Institutes, Japan, paper No. 1053 (1967)

(8) G. Quilico; CIGRÉ Report No. 214 (1956)

(9) G. Quilico; L'Elettrotecnica vol. XLI No. 10 pp. 530-538 (1954)